17

Energy Transfer from Silicon Nanocrystals to Er^{3+} Ions Embedded in Silicon Oxide Matrix

Kantisara Pita and Quang Vinh Vu
Photonic Research Centre, School of Electrical and Electronics Engineering, Nanyang Technological University, 50 Nanyang Avenue
CINTRA CNRS/NTU/THALES, UMI 3288, Research Techno Plaza, 50 Nanyang Drive, Border X Block, Level 6
Singapore

1. Introduction

Silicon (Si) based light emitting devices have drawn much attention for the integration of electronic and photonics. Si nanostructures (amorphous clusters or crystals) have been recognized as good candidates for effective light emitting devices (Bulutay, 2007; Seino et al., 2009; Takagahara & Takeda, 2007; Wolkin et al., 1999). However, photons emitted by Si nanostructures can be reabsorbed by Si waveguides due to the higher photon energy compared to bulk Si bandgap. To overcome this problem, Erbium (Er) doped Si nanostructures embedded in SiO_2 matrix has been extensively studied (Fujii et al., 2004; Heitmann et al., 2003; Kik & Polman, 2001; Polman & Veggel, 2004; Savchyn et al., 2007, 2008). Si nanostructures can be excited optically or electrically, then transfer the energy to Er^{3+} ions which then decay radiatively giving emission peaked at 1.53μm, which coincides with the telecommunication wavelength. Hence, light sources made by this material system (Er^{3+} ions doped Si nanostructures embedded in SiO_2 matrix) in the integrated Si platforms can be used directly with telecommunication devices.

To date, however, one of the main challenges of this material system is the low energy transfer efficiency from Si nanostructures to Er^{3+} ions, which we are going to address in this chapter. To increase the energy transfer efficiency, the mechanism of the energy transfer must be well understood. Prior to 2007, many research works reported that the main energy transfer mechanism is from Si nanocrystals to Er^{3+} ions (Fujii et al., 2004; Heitmann et al., 2003; Kik & Polman, 2001; Polman & Veggel, 2004). However, recently, in 2007 and 2008, one leading group in the field suggested that defect mediated energy transfer was the dominant mechanism (Savchyn et al., 2007, 2008). In their work (Savchyn et al., 2007, 2008), the origin of defects that transfer energy to Er^{3+} ions was not discussed. The controversial in the energy transfer mechanism has created much difficulty in improving Er^{3+} emission efficiency. The approach to improve Er^{3+} emission efficiency will clearly very much depend on the dominant mechanism of the energy transfer to Er^{3+} ions, whether the defects or the Si nanocrystals are the dominant factor for the energy transfer.

In this chapter, we present our work on different energy transitions from defects and from Si nanocrystals and their energy transfer efficiency to Er^{3+} ions. Bulk Silicon Rich Oxide

(SRO) and alternate layers of SRO and SiO_2 films (SRO/SiO_2 superlattice) with and without Er^{3+} ions incorporation were developed by co-sputtering method. Through the photoluminescence (PL) study of the samples annealed at temperature ranging from 500°C to 1050°C, with and without passivation (further annealing in a forming gas of 5% H_2 and 95% N_2 mixture), 4 different energy transitions and their energy transfer to Er^{3+} ions have been identified and investigated. Optimum Er^{3+} ions concentration for maximized Er^{3+} emission in superlattice structure has also been found. Through the lifetime measurement, transfer rate and transfer efficiency from exciton recombination in Si nanocrystals to Er^{3+} ions in our superlattice structure have also been found.

2. Preparation of Si nanostructures embedded in SiO_2 matrix with/without Er^{3+} ions incorporation by co-sputtering deposition method

In this section, the preparation of Si nanostructures embedded in SiO_2 matrix is described. The substrates were 4'' Si wafers which were cleaned from dust particles by blowing with a nitrogen gun before loaded into a sputtering deposition chamber. Co-sputtering method was chosen as deposition method due to its flexibility to incorporate different species into the films and the well-controlled deposition rate.

Before depositing the films, the chamber was pumped down to a pressure of ~5×10^{-6} torr. The substrate holder was then heated to temperature of 250°C for 1 hour to outgas the substrates. All depositions were carried out at the base pressure of ~5×10^{-7} torr and substrate temperature of 100°C using an Argon gas with a pressure of ~6.3×10^{-3} torr. To ensure uniformity, the substrate was rotated at 20rpm. Prior to each deposition, the targets were pre-sputtered at low power (20W) for 15 minutes to ensure each target was free of surface contamination.

SiO_2 layers were deposited by sputtering a SiO_2 target. To deposit Silicon Rich Oxide (SRO) layers, a SiO_2 target and a Si target were co-sputtered simultaneously. The concentration of Si in SRO layers can be controlled by controlling the power of each target. To incorporate Er^{3+} ions into the films, an Er_2O_3 target was co-sputtered simultaneously. Generally, the Er^{3+} ions are incorporated using the ion implantation technique (Castagna et al., 2003, 2006; Heitmann et al., 2003; Iacona et al., 2006). The use of the co-sputtering method to incorporate Er^{3+} ions has two major advantages: (i) the ability to control the locations of Er^{3+} ions and (ii) no extra defects are introduced which has to be cured by a post annealing process. The ability to control location of Er^{3+} ions is important because the energy transfer to Er^{3+} ions can only be achieved when the donors and acceptors are close to each other (Heitmann et al., 2003). In our process, the deposition rates for SiO_2 and SRO layers are 4.5nm/minute and 8nm/minute, respectively. These slow deposition rates have enabled us to accurately control the layer thickness of few nm.

To study the mechanism of different energy transitions and their energy transfer to Er^{3+} ions, bulk SRO and alternate layers of SRO and SiO_2 films (SRO/SiO_2 superlattice) with and without Er^{3+} ions incorporation were deposited and annealed at different temperatures. The bulk SRO samples with and without Er^{3+} ions incorporation are, respectively, referred to as SRO and Er^{3+}:SRO samples, and the SRO/SiO_2 superlattice samples with and without Er^{3+} ions incorporation are, respectively, referred to as SRO/SiO_2 and Er^{3+}:SRO/SiO_2 samples. Figure 1 shows the cross section of bulk SRO and Er^{3+}:SRO structure. The Si concentration in SRO layer was 52 at%. Figure 2 shows the cross section of SRO/SiO_2 and Er^{3+}:SRO/SiO_2 superlattice structure.

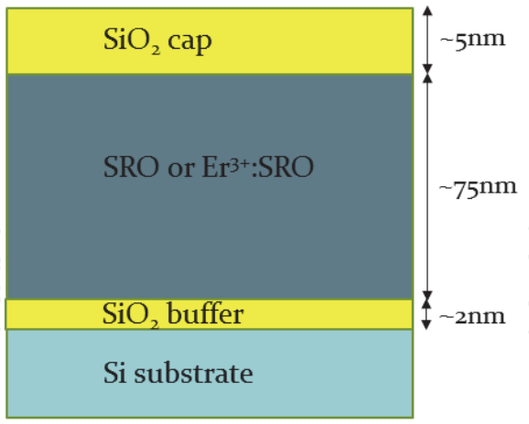

Fig. 1. Cross section of the bulk SRO and Er^{3+}:SRO samples deposited by the co-sputtering process

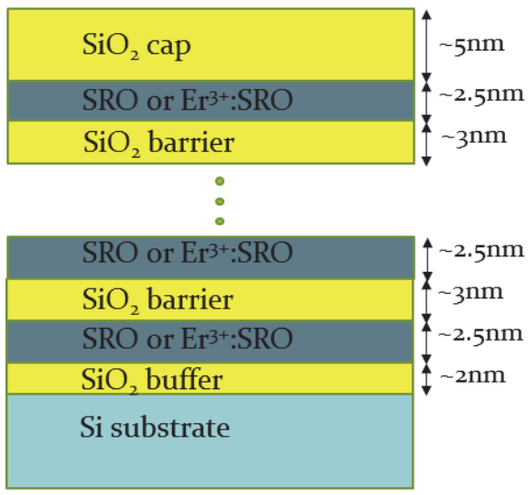

Fig. 2. Cross section of the SRO/SiO_2 and Er^{3+}:SRO/SiO_2 superlattice samples deposited by the co-sputtering process

Similar to bulk SRO, the Si concentration in each SRO layer of SRO/SiO_2 superlattice was 52 at%. The number of SRO layers in these sample was 30, making total thickness of SRO layers 75nm, which is the same as that of the bulk samples.

All bulk and superlattice samples were annealed using a rapid thermal processor (RTP) at various temperatures. Prior to each annealing process, the RTP chamber was vacuum pumped and then filled with nitrogen in several cycles to minimize the presence of oxygen in annealing chamber. All annealing processes were done in nitrogen environment. The annealing temperature ranged from 500°C to 1050°C. The annealing time was fixed at 1 minute.

After the annealing process, some of the samples were passivated. The passivation process was done by annealing the samples in a forming gas (H_2 5% N_2 95%) at 500°C. The samples annealed by the RTP only are referred to as "as-annealed" samples and the samples annealed by the RTP and passivated are referred to as "passivated" samples. The purpose of

the passivation is to remove the dangling bond defects surrounding Si nanostructures (Savchyn et al., 2008; Wilkinson & Elliman, 2003). In our study, we have varied the passivation time and found that after 30 minutes of the passivation, the emission intensity of exciton recombinations in Si nanocrystals as well as the exciton lifetime have reached the optimum values and saturated, showing that most, if not all, dangling bond defects have been effectively removed. To ensure that we remove most, if not all, dangling bond defects, we passivated our samples for 1 hour.

In our work, we also varied the concentrations of Er^{3+} ions to obtain the optimum Er^{3+} ion concentration, the energy transfer rate and the transfer efficiency to Er^{3+} ions for our materials system. The samples were prepared using similar structure as shown in Figure 2. The samples were annealed at 1050°C in N_2 ambience for 1 minute and then passivated at 500°C in forming gas for 1 hour. Er^{3+} ion concentration was varied from 0.02 at% to 0.4 at% by varying the Er_2O_3 deposition power from 5W to 35W.

To study different energy transitions from defects and from Si nanocrystals and their energy transfer efficiency to Er^{3+} ions, photoluminescence (PL) was performed on the as-annealed and passivated SRO, Er^{3+}:SRO, SRO/SiO_2, and Er^{3+}:SRO/SiO_2 samples. The PL spectra of all samples were taken using a Fluorolog-3 system. Excitation is fixed at 290nm by using a Xenon lamp and a monocromator. The spectra are corrected to the respond of the detector. All PL measurements were done at room temperature. Two detection ranges were investigated: (i) visible to near Infra-Red (IR) (400nm-850nm) to study emission from different kinds of defects and from exciton recombinations in Si nanocrystals and (ii) IR range (1470nm-1700nm) to detect the Er^{3+} emission peaked at 1535nm. The lifetime was measured using the same Fluorolog-3 system with a Xenon flash lamp. The transmission electron microscopy (TEM) was used to characterize the Si nanostructure in our samples. The concentrations of excess Si and Er^{3+} ions in our samples was estimated by the deposition rate of each target at each deposition power.

3. Si nanocrystals, different kinds of defects in bulk & superlattice structures and their energy transfer to Er^{3+} ions

3.1 TEM images of samples

Figure 3 shows TEM images of the bulk SRO samples annealed at 850°C and 950°C and the SRO/SiO_2 superlattice sample annealed at 950°C respectively.

As shown in Figure 3 (a), at the annealing temperature of 850°C, there are amorphous Si nanostructures, shown in the TEM image as dark coloured patches, in the bulk SRO sample. For our SRO/SiO_2 superlattice samples, it has been established through a TEM image that at the annealing temperature of 850°C, similar to our bulk samples, there are only amorphous Si nanostructures in the SRO/SiO_2 superlattice samples developed by our group (Silalahi et al., 2010). Up to 850°C annealing temperature, there is no crystallization of Si can be observed in both our bulk SRO and SRO/SiO_2 samples. On the other hand, at the annealing temperature of 950°C, as shown in Figures 3 (b) and (c) respectively, the fringes of Si nanocrystals can be clearly observed in both the bulk SRO sample and the SRO/SiO_2 superlattice sample. These results shows that in our samples, the nanocrystals have been formed at the annealing temperature of 950°C while at the annealing temperature of 850°C, the Si nanostructures are still in an amorphous state.

From Figure 3 (b), the diameter of Si nanocrystals in the bulk SRO sample ranges from 2.7nm to 4.2nm with an average of 3.3nm. In the SRO/SiO_2 superlattice sample, from Figure

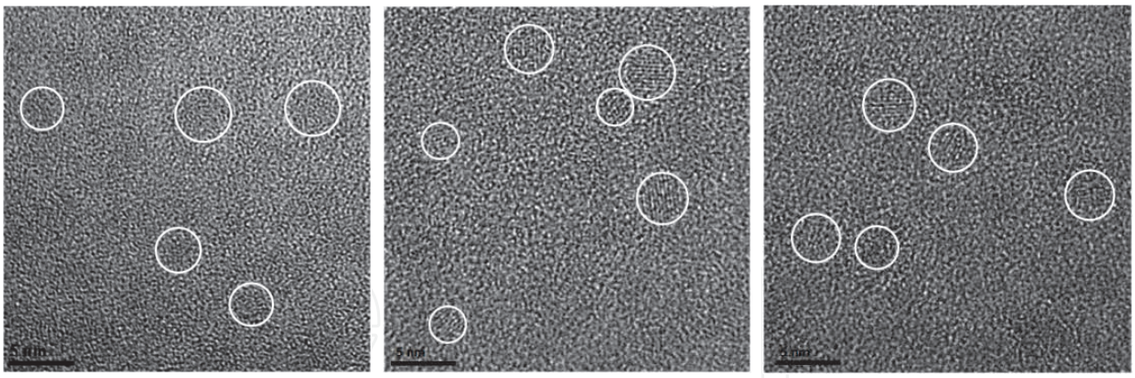

(a) (b) (c)

Fig. 3. TEM images of (a) the bulk SRO sample annealed at 850°C, (b) the bulk SRO sample annealed at 950°C, and (c) the SRO/SiO_2 superlattice sample annealed at 950°C

3 (c), the diameter of Si nanocrystals ranges from 3.3nm to 3.9nm with an average of 3.6nm. The TEM images show that the size distribution of Si nanocrystals in the bulk sample is larger than that in the superlattice sample. Indeed, the aim of using the superlattice structure is to have better control on the size of Si nanocrystals.

3.2 Visible to near IR PL (400nm-850nm) of the bulk SRO and Er^{3+}:SRO samples

Visible to near IR PL spectra of the as-annealed and passivated bulk SRO and Er^{3+}:SRO samples annealed at different temperature are shown in Figure 4 (a) and Figure 4 (b) respectively.

In Figures 4(a) and 4(b), we observe that there are two PL emission bands peaked at ~570nm and ~800nm. First of all, let us consider the emission peaked at ~800nm.

At the annealing temperature lower than 950°C, the emission at ~800nm is not observed in any of our samples. At the annealing temperature of 950°C, the emission at ~800nm is only detected from the passivated SRO and Er^{3+}:SRO samples. For the as-annealed bulk SRO and Er^{3+}:SRO samples, this emission is very low, almost not observable. At the annealing temperature of 1050°C, all of the as-annealed and passivated bulk SRO and Er^{3+}:SRO samples have emission peaked at ~800nm. It has been established that, for our samples, Si nanocrystals have been formed when the samples were annealed at 950°C (see Figure 3 (b) in section 3.1 above). The emission peaked at ~800nm can only be observed when Si nanocrystals are present in the samples and is attributed to the exciton recombinations in Si nanocrystals (Bulutay, 2007; Charvet et al., 1999; Kik & Polman, 2001; Seino et al., 2009; Silalahi et al., 2009, 2010; Wilkinson & Elliman, 2003). The increase of the emission intensity at the higher annealing temperature (in our case, 1050°C compared to 950°C) has also been reported and attributed to the better crystallization of Si nanocrystals (Kahler & Hofmeister, 2002; Kapaklis et al., 2005).

At the annealing temperature of 1050°C, the intensity of the ~800nm emission from the passivated samples are more than 4 times higher than that from the as-annealed samples. The increase of this emission upon passivation is due to the removal of dangling bond defects, which introduce non-radiative paths that quenches the radiative excitation recombinations in Si nanocrystals (Savchyn et al., 2008; Wilkinson & Elliman, 2003). For the 950°C as-annealed SRO and Er^{3+}:SRO samples, the emission from the exciton recombinations in Si nanocrystals is effectively quenched by the dangling bond defects.

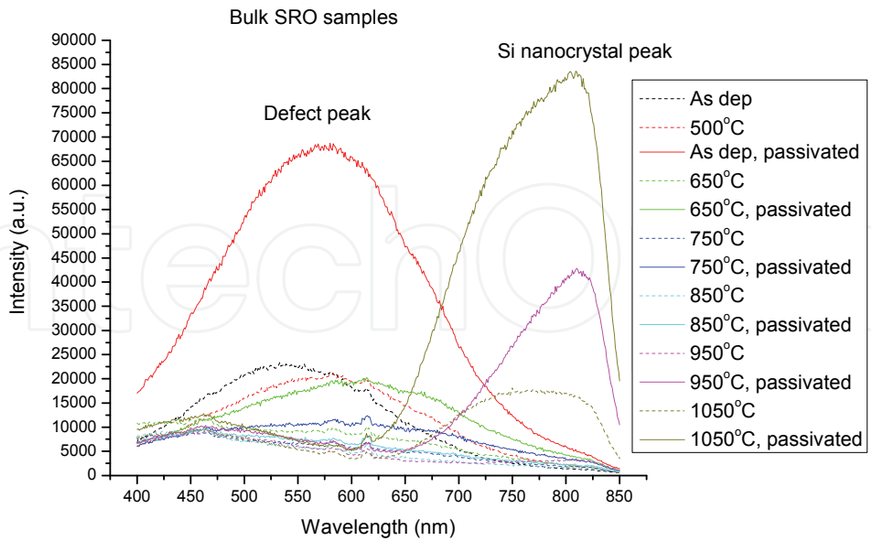

(a)

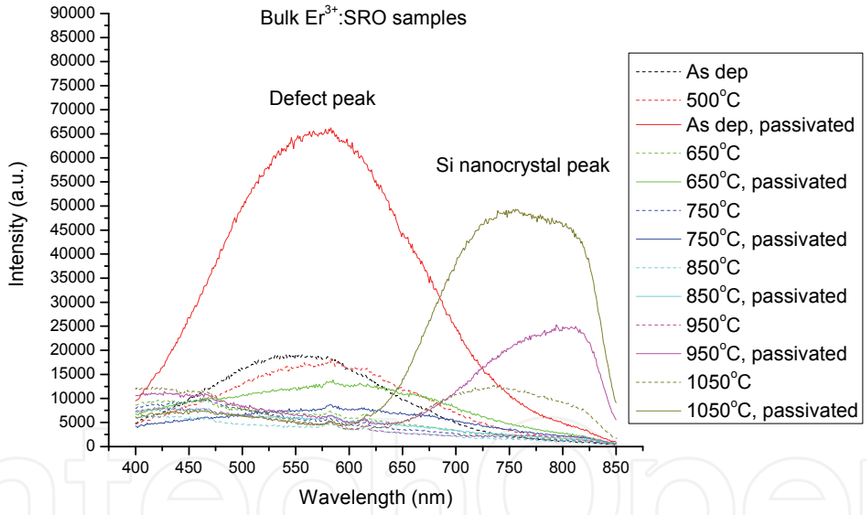

(b)

Fig. 4. Visible to near IR PL spectra of (a) the bulk SRO samples and (b) the bulk Er^{3+}:SRO samples at different annealing temperature under the excitation of 290nm

Upon passivation, where most dangling bond defects have been removed, the emission from exciton recombinations in Si nanocrystals can then be clearly observed.

From Figures 4 (a) and (b), we notice that the emission intensity at ~ 800nm of the bulk Er^{3+}:SRO samples is lower than that of the bulk SRO samples undergoing the same heat treatment and passivation. Furthermore, we also observe that the Er^{3+}:SRO samples have emission peaked at 1535nm due to the transition from excited state $^4I_{13/2}$ to ground state $^4I_{15/2}$ in the Er^{3+} ions (the emission spectra of the Er^{3+} ions will be presented in Figure 8 (a) in

section 3.4 below). The decrease of the emission intensity due to the exciton recombinations in Si nanocrystals and the presence of Er^{3+} emission, upon Er^{3+} ions incorporation, is an indication of an energy transfer from the exciton recombinations in Si nanocrystals to Er^{3+} ions. When Er^{3+} ions are near a Si nanocrystal, excitons in the Si nanocrystal can recombine non-radiatively, transfer their energies to the Er^{3+} ions and excite them. The excited Er^{3+} ions can then decay radiatively from $^4I_{13/2}$ to $^4I_{15/2}$, giving emission peak at 1535nm. This energy transfer mechanism has been reported earlier (Fujii et al., 2004; Heitmann et al., 2003; Kik & Polman, 2001; Polman & Veggel, 2004). The efficiency of energy transfer from exciton recombinations in Si nanocrystals to Er^{3+} ions will be discussed in more detail in section 3.4.
Now, let us consider the emission at ~570nm. As shown in Figure 4 (a) and (b), for both bulk SRO and Er^{3+}:SRO, the as-deposited samples and the samples annealed at low temperature (500°C - 650°C) show a dominant emission peaked at ~570nm. To investigate the evolution of this emission, the peak intensity at 570nm of the as-annealed and passivated SRO and Er^{3+}:SRO samples was plotted as a function of the annealing temperature, as shown in Figure 5.

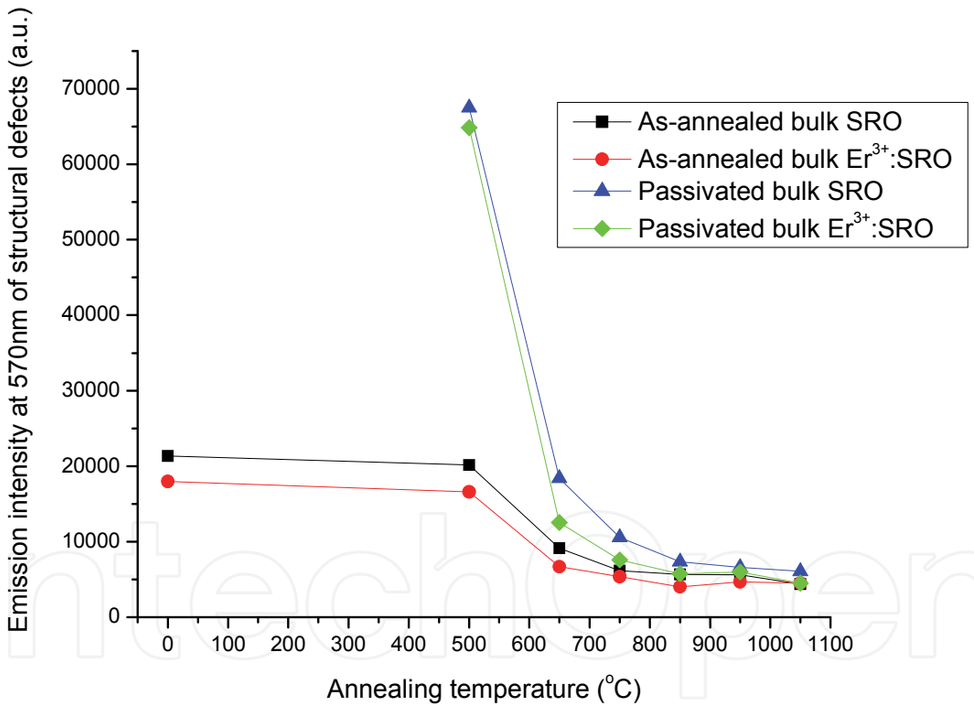

Fig. 5. Evolution of the emission peak at 570nm of the as-annealed and passivated SRO and Er^{3+}:SRO samples as a function of the annealing temperature

From Figure 5, we notice that for the as-annealed SRO and Er^{3+}:SRO samples, the emissions peaked at ~570nm are almost constant from the as-deposited samples up to the post-deposition annealing temperature of 500°C. The emissions then decrease beyond 500°C annealing temperature. We also observe that the emissions from the passivated SRO and Er^{3+}:SRO samples annealed at 500°C are significantly higher than those as-annealed samples

and then reduce to the level comparable to the as-annealed samples beyond 500°C annealing temperature. The reduction of the emissions from all the samples at the annealing temperature higher than 500°C (i.e. the emissions decrease with the formation of Silicon amorphous nanostructures and nanocrystals) indicates that these emissions must be due to the defects rather than the Silicon amorphous nanostructures or nanocrystals. Furthermore, the reason that the emissions from the passivated SRO and Er^{3+}:SRO samples are significantly higher than those from the as-annealed SRO and Er^{3+}:SRO samples is because the passivation processes have removed the dangling bond defects which can serve as the non-radiative recombination path. Consequently, this emission which we have attributed to the defects must be due to the structural defects, associated with the presence of rich Silicon atoms and cannot be removed by the passivation process.

In Figure 5, we also see that emissions from Er^{3+}:SRO samples for both the as-annealed and passivated samples are consistently lower than those from just SRO samples. This is due to the energy transfer from those defects to excite the Er^{3+} ions which in turn give emission peaked at ~1535nm. We have indeed obtained the Er^{3+} emissions from our Er^{3+}:SRO samples annealed at 500°C, which are shown in Figure 8 (a). The efficiency of these defects on energy transfer to Er^{3+} ions will be discussed in detail in section 3.4.

3.3 Visible to near IR PL (400nm-850nm) of the SRO/SiO_2 superlattice and Er^{3+}:SRO/SiO_2 superlattice samples

Visible to near IR PL spectra of the as-annealed and passivated SRO/SiO_2 and Er^{3+}:SRO/SiO_2 superlattice samples annealed at different temperature are shown in Figure 6 (a) and Figure 6 (b) respectively.

As shown in Figures 6 (a) and (b), at the annealing temperature of 950°C and 1050°C, all SRO/SiO_2 and Er^{3+}:SRO/SiO_2 samples show the emission from the exciton recombinations in Si nanocrystals at ~800nm. Recall that, in section 3.2 above, the emission from the exciton recombinations in Si nanocrystals is not observed in the as-annealed bulk SRO and Er^{3+}:SRO samples annealed at 950°C. The appearance of this emission in the as-annealed SRO/SiO_2 and Er^{3+}:SRO/SiO_2 samples annealed at 950°C suggests that the superlattice structure has induced better crystallization. Similar to the bulk SRO and Er^{3+}:SRO samples, the emission intensity at ~800nm of the SRO/SiO_2 and Er^{3+}:SRO/SiO_2 samples annealed at 1050°C is higher than that of the samples annealed at 950°C. Furthermore, the intensity of this emission increases upon passivation. Again, as discussed above, the higher emission intensity at the annealing temperature of 1050°C is due to better crystallization of the Si nanocrystals and the increase of intensity upon passivation is the result of dangling bond defects removal. Also similar to the bulk SRO and Er^{3+}:SRO samples, the decreases of the exciton recombination emission intensity with the presence of Er^{3+} ions in the Er^{3+}:SRO/SiO_2 superlattice samples indicates energy transfer from the exciton recombinations in Si nanocrystals to Er^{3+} ions.

We observe that the as-deposited SRO/SiO_2 and Er^{3+}:SRO/SiO_2 samples and those annealed at low temperature (500°C-650°C) show an emission peaked at ~500nm. The peak intensity at 500nm of this emission was plotted as a function of the annealing temperature and is shown in Figure 7.

As shown in Figure 7, the emission of the as-deposited samples is just slightly higher than that of the as-annealed samples annealed at 500°C. Above 500°C, the emissions of the as-annealed and passivated SRO/SiO_2 and Er^{3+}:SRO/SiO_2 samples decrease. The decrease of this emission with the increasing annealing temperature indicates that this emission is

originated from defects. Furthermore, all the passivated SRO/SiO_2 and Er^{3+}:SRO/SiO_2 samples show a significantly higher emission intensity than that of the as-annealed samples. As in the case of the bulk samples discussed above, this simply indicates that the dangling bonds, which can serve as non-radiative recombination path, have been removed by the

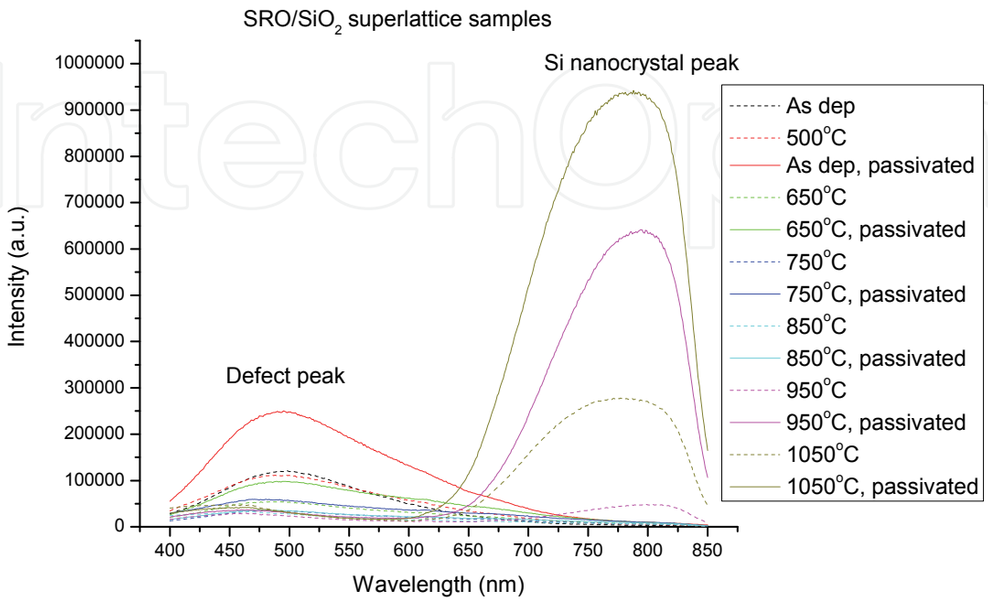

(a)

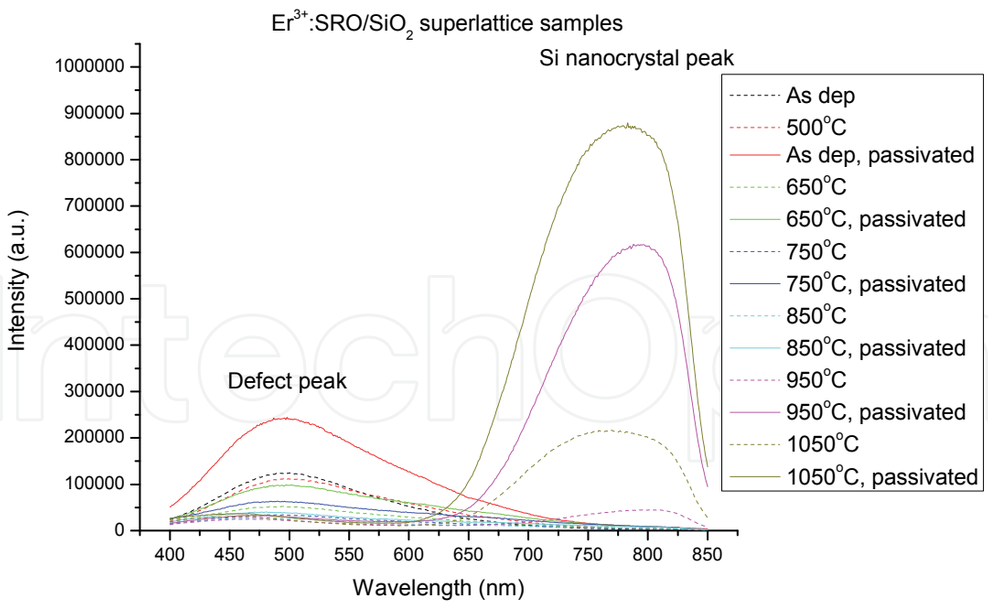

(b)

Fig. 6. Visible to near IR PL spectra of (a) the SRO/SiO_2 superlattice samples and (b) the Er^{3+}:SRO/SiO_2 superlattice samples at different annealing temperature under the excitation of 290nm

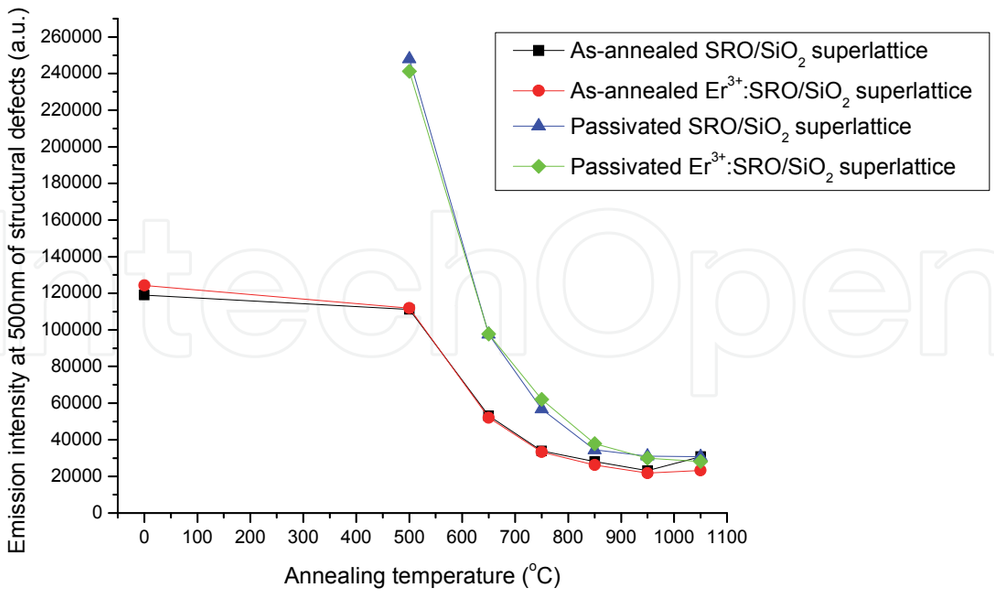

Fig. 7. Evolution of the emission peak at 500nm of the as-annealed and passivated SRO/SiO_2 and Er^{3+}:SRO/SiO_2 superlattice samples as a function of the annealing temperature

passivation. Since this defect related emission is only observed in the superlattice samples, the defects are most likely formed by structural defects that only occur in superlattice structure. The stress between SRO (or Er^{3+}:SRO) layers and SiO_2 layers may presumably induce such defects. In contrast to the defect emission of the bulk samples presented in Section 3.2, we notice here that the emission intensity of the SRO/SiO_2 samples are practically the same as that of the Er^{3+}:SRO/SiO_2 samples under the same annealing conditions. This suggests that these defects are not transferring their energy to Er^{3+} ions. Accordingly, as shown later in section 3.4, we indeed could not observe the emission of Er^{3+} ions due to the energy transfer from these defects.

We have observed from the PL spectra above that there is no emission that can be attributed to dangling bond defects. An emission due to dangling bond defects is expected to decrease with the passivation. For all of our samples, all detected PL emissions increases with the passivation. In the literature, no emission linked to dangling bond defects was reported either in visible or in IR range (Polman & Veggel, 2004; Savchyn et al., 2008; Silalahi et al., 2010; Wilkinson & Elliman, 2003). Up to this point, we conclude that dangling bond defects can serve as non-radiative de-excitation paths competing with and quenching other radiative de-excitation processes. However, in our study, from the emission intensity of Er^{3+} ions of the as-annealed and passivated Er^{3+}:SRO/SiO_2 superlattice samples presented in section 3.4 below, we observe that dangling bond defects may transfer their energy to Er^{3+} ions. This energy transfer mechanism and its efficiency will be discussed in detail in section 3.4.

3.4 IR (1470nm-1700nm) PL of the bulk Er^{3+}:SRO and Er^{3+}:SRO/SiO_2 superlattice samples

In section 3.2 and 3.3, four energy transitions have been identified: i) the emission of exciton recombinations in Si nanocrystals, ii) the non-radiative dangling bond de-excitation, iii) the

emission from the structural defects in bulk structure, and iv) the emission from the structural defects in superlattice structure. In this section, the IR spectra at 1470nm-1700nm of the bulk Er^{3+}:SRO and Er^{3+}:SRO/SiO_2 superlattice samples will be presented and discussed to provide deeper understanding on the efficiency of those energy transitions in transferring energy to Er^{3+} ions.

Figure 8 (a) shows IR PL spectra from 1470nm to 1700nm of the bulk Er^{3+}:SRO samples. The emission peak at 1535nm is the well-known radiative transition from excited level $^4I_{13/2}$ to ground state $^4I_{15/2}$ of Er^{3+} ions, which has been reported earlier (Castagna et al., 2003, 2006; Heitmann et al., 2003; Iacona et al., 2006; Polman & Veggel, 2004; Savchyn et al., 2007). In this chapter, the emission peak at 1535nm will be referred to as "Er^{3+} peak". Figure 8 (b) shows the evolution of Er^{3+} peak intensity at 1535nm as a function of the annealing temperature of the as-annealed and passivated bulk Er^{3+}:SRO and Er^{3+}:SRO/SiO_2 superlattice samples. The excitation was fixed at 290nm.

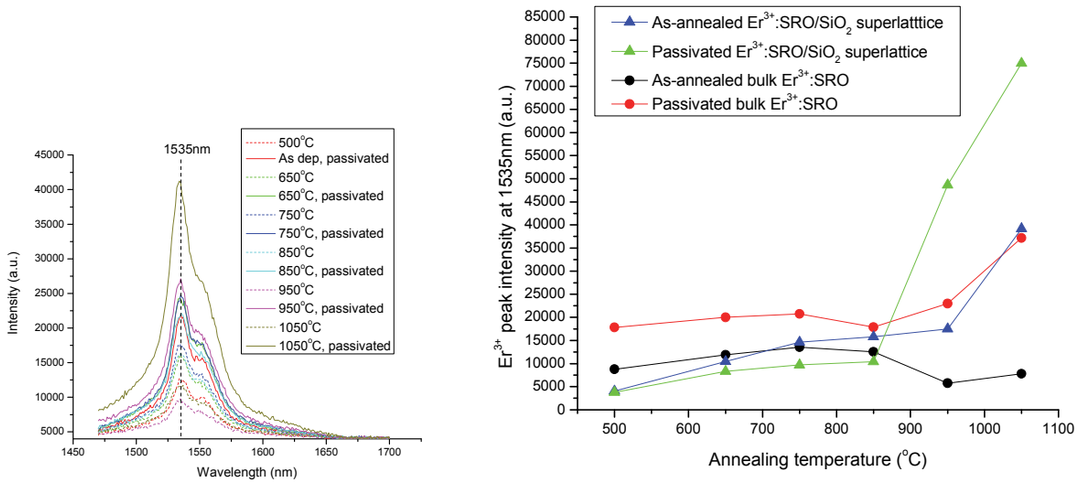

(a) (b)

Fig. 8. (a) IR PL spectra at 1470nm-1700nm of the bulk Er^{3+}:SRO samples (b) Evolution of the Er^{3+} peak intensity at 1535nm as a function of the annealing temperature of the as-annealed and passivated bulk Er^{3+}:SRO and Er^{3+}:SRO/SiO_2 superlattice samples. The excitation was fixed at 290nm

Let us firstly analyse the Er^{3+} emission intensity of the as-annealed and passivated Er^{3+}:SRO/SiO_2 superlattice samples at the annealing temperature from 500°C to 850°C (respectively, blue and green curves in Figure 8 (b)). At these annealing temperatures, the Si nanocrystals have not been formed (Silalahi et al., 2010) and consequently the emission from the exciton recombinations in Si nanocrystals at ~800nm is absent (see Figures 6 (b)). The excitation leading to the emission of Er^{3+} ions is from the energy transfer from defects. As discussed in section 3.3 above, the structural defects in superlattice structure, which gives emission at ~500nm, cannot transfer energy to Er^{3+} ions. Hence, the excitation of Er^{3+} ions is likely from the dangling bond defects. Indeed, upon passivation, which removes the dangling bond defects, the Er^{3+} peak intensity reduces. The decrease of Er^{3+} peak intensity after passivation has also been reported in similar material system (Silalahi et al., 2010).

At the annealing temperature of 950°C and above, Si nanocrystals have been formed in the Er^{3+}:SRO/SiO_2 superlattice samples (see Figure 3 (c)). Before the passivation, the exciton recombinations in Si nanocrystals are quenched by the dangling bond defects (see Figure 6 (b)). The energy transfer to Er^{3+} ions can be from both the exciton recombinations in Si nanocrystals and the dangling bond defects. When the dangling bond defects are removed by the passivation, the Er^{3+} peak intensity is about two times of that of the as-annealed samples (see, respectively, the green and blue curves in Figure 8 (b)). The exciton recombinations in the Si nanocrystals are no longer quenched by the dangling bond defects and, of course, the energy transfer from the dangling bond defects to Er^{3+} ions have also been mostly suppressed, leaving only energy transfer from the exciton recombinations in Si nanocrystals to Er^{3+} ions. The dramatic increase in the Er^{3+} peak intensity shows that the exciton recombinations in Si nanocrystals are much more efficient than the dangling bond defects in transferring their energy to Er^{3+} ions.

Next, let us consider the Er^{3+} emission intensity of the as-annealed and passivated bulk Er^{3+}:SRO samples (respectively, black and red curves in Figure 8 (b)). Again, at the annealing temperature equal or lower than 850°C, Si nanocrystals have not been formed (see Figure 3 (a)) and so the excitation of Er^{3+} ions must consequently be due to the energy transfer from the defects. Before the passivation, where both the structural defects and the dangling bond defects are present, the energy transfer to Er^{3+} ions can be from both of these defects. After the passivation, the dangling bond defects have been removed, and therefore the Er^{3+} ion excitation is dominated by the energy transfer from the structural defects. It is observed that after the passivation, the Er^{3+} peak intensity is ~2 times of that of the as-annealed samples (see, respectively, red and black curves in Figure 8 (b)). The increase of the Er^{3+} peak intensity upon passivation shows that the structural defects are more efficient than the dangling bond defects in transferring energy to Er^{3+} ions.

At the annealing temperature higher than 850°C, the structural defects in the bulk Er^{3+}:SRO samples have been suppressed (see Figure 5) and the Si nanocrystals have been formed (see Figure 3 (b)). Upon passivation, as the dangling bond defects have been removed, the energy transfer to Er^{3+} ions is dominated by the exciton recombinations in Si nanocrystals. The Er^{3+} peak intensity of the passivated Er^{3+}:SRO samples becomes ~4 times of that of the as-annealed samples (see, respectively, red and black curves in Figure 8 (b)). It is important to note that the Er^{3+} peak intensity of the passivated bulk Er^{3+}:SRO samples annealed at temperature higher than 850°C, where the energy transfer to Er^{3+} ions is dominated by the exciton recombinations in Si nanocrystals, is up to ~2 times higher than that of the passivated bulk Er^{3+}:SRO samples annealed at temperature below 850°C, where the energy transfer to Er^{3+} ions is dominated by the structural defects in bulk structure. This implies that the exciton recombinations in Si nanocrystals are more efficient than the bulk structural defects in transferring their energy to Er^{3+} ions.

Comparing the passivated bulk Er^{3+}:SRO and the passivated Er^{3+}:SRO/SiO_2 superlattice samples at the annealing temperature higher than 850°C (respectively, red and green curves in Figure 8 (b)), where the energy transfer is dominated by the exciton recombinations in Si nanocrystals, the Er^{3+} peak intensity of the superlattice samples is more than 2 times higher than that of the bulk samples. One possible explanation is a better size control of Si nanocrystals in superlattice structure compared to the bulk structure (Gourbilleau et al., 2001; Zacharias et al., 2002). As the energy can be transferred from smaller nanocrystals to larger nanocrystals (Iwayama et al., 1999), a better size control may then suppress this

energy transfer and hence remove a competitive recombination path of energy transfer to Er^{3+} ions, leading to a more efficient energy transfer to Er^{3+} ions.

Based on the above discussion, we summarize schematically the energy transitions of the exciton recombinations in Si nanocrystal, the structural defects in the bulk Er^{3+}:SRO samples, the structural defects in the Er^{3+}:SRO/SiO_2 superlattice samples, the dangling bond defects and their energy transfer to Er^{3+} ions in Figure 9.

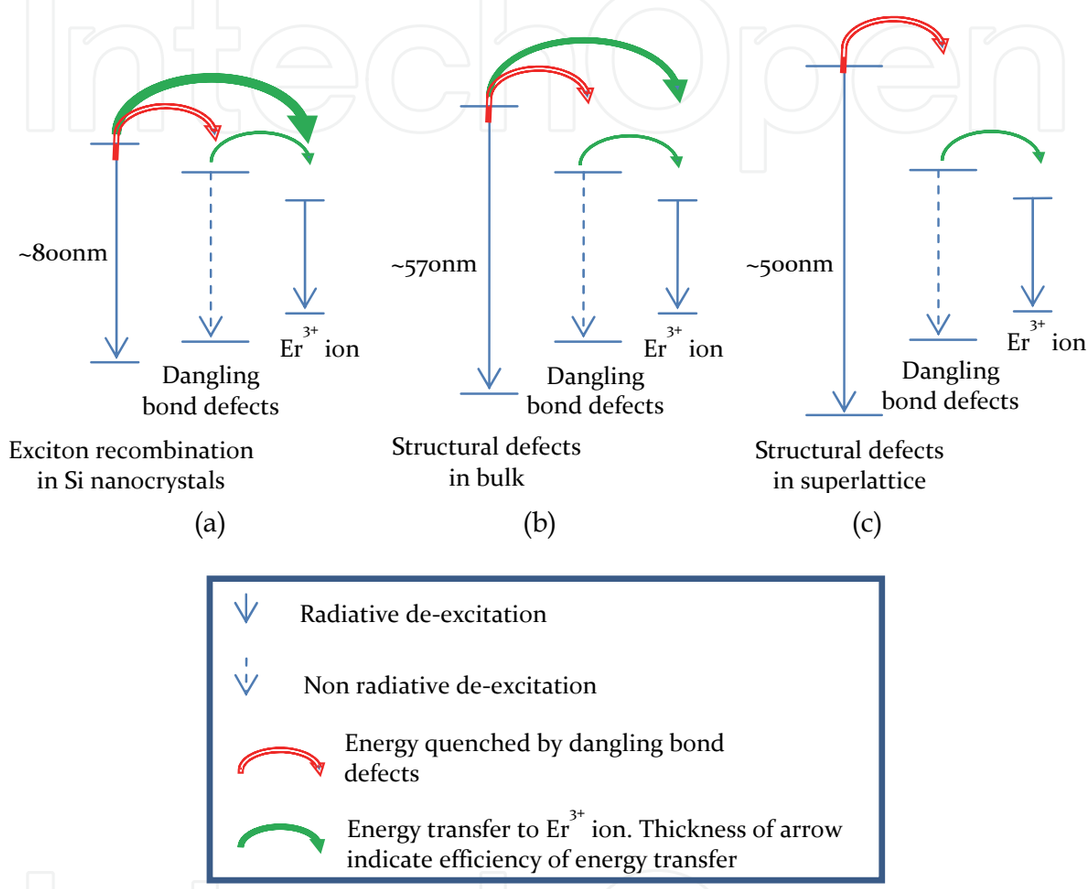

Fig. 9. Different energy transitions and their energy transfer to Er^{3+} ions

Figure 9 (a) shows the exciton radiative recombination, which gives emission at ~800nm, and the energy transfer from the exciton recombination in Si nanocrystals to Er^{3+} ions. The dangling bond defects not only create non-radiative de-excitation paths that quench the exciton recombination in Si nanocrystals, but also transfer their energy to Er^{3+} ions with efficiency much lower than that of the exciton recombination in Si nanocrystals. Figure 9 (b) shows the radiative de-excitation of the structural defects in the bulk Er^{3+}:SRO samples, which gives emission at ~570nm, and their energy transfer to Er^{3+} ions. Note that the energy transfer efficiency from these defects to Er^{3+} ions is lower than that of the exciton recombination in Si nanocrystals. The dangling bond defects create non-radiative de-excitation paths and transfer their energy to Er^{3+} ions with efficiency lower than that of these structural defects. In Figure 9 (c), the structural defects in the Er^{3+}:SRO/SiO_2 superlattice samples show the radiative de-excitation responsible for emission at ~500nm. These defects

do not transfer energy to Er^{3+} ions. Similar to the transitions described in Figures 9 (a) and (b), the dangling bond defects create non-radiative de-excitation paths and transfer their energy to Er^{3+} ions. When most defects have been reduced by the high temperature annealing and the passivation, the exciton recombinations in Si nanocrystals in the Er^{3+}:SRO/SiO_2 superlattice samples are more efficient than that in the bulk Er^{3+}:SRO samples in transferring their energy to Er^{3+} ions.

4. Er^{3+} ion concentration effect on Er^{3+} emission in superlattice structure

It has been shown in previous section that the exciton recombinations process in Si nanocrystals in our passivated superlattice samples is the most efficient in energy transfer to Er^{3+} ions. Therefore, in this section, to study the effect of Er^{3+} ion concentration on Er^{3+} emission, we have used Er^{3+}:SRO/SiO_2 superlattice samples annealed at 1050°C and passivated.

4.1 Optimization of Er^{3+} ion concentration

The optimization of Er^{3+} ion concentration was carried out by varying the Er_2O_3 deposition power from 5W to 35W, resulting Er^{3+} ion concentration from 0.02 at% to 0.4 at%. Figure 10 shows the variation of the exciton recombination peak intensities at ~800nm and the Er^{3+} peak intensities at 1535nm with the Er^{3+} ion concentration and the ratio of Er^{3+} ions to the number of Silicon nanocrystals. The ratio of Er^{3+} ions to the number of Silicon nanocrystals is obtained using the concentration of Er^{3+} ions and concentration of Si nanocrystals assuming Si nanocrystals average size of 3.6nm (see section 3.1).

As shown in Figure 10, as the Er^{3+} ion concentration increases, the peak intensity of the exciton recombinations in Si nanocrystals decreases continuously. With increasing number of Er^{3+} ions in the samples, the mean distance between Er^{3+} ions and Si nanocrystals decreases, and so stronger coupling between the two species is expected. The shorter distance to the Er^{3+} ions together with the increasing Er^{3+} ion concentrations make the excitons in Si nanocrystals more likely to recombine non-radiatively and transfer their energy to Er^{3+} ions (Heitmann et al., 2003). Hence, the emission from the exciton recombination Si nanocrystals is quenched with increasing Er^{3+} ion concentration. We would expect that when all the excitons in Si nanocrystals transfer their energy to Er^{3+} ions, we could no longer detect the emission from exciton recombination in Si nanocrystals. For our samples, this occurs when the concentration of Er^{3+} ions reach 0.27 at%, which corresponds to Er^{3+} ions to the number of Silicon nanocrystals ratio of 13. Although, at this Er^{3+} ion concentrations, all the excitons in Si nanocrystals have apparently transferred their energy to Er^{3+} ions, it does not mean that it would give the maximum optimum Er^{3+} emission intensity as we will discuss below.

In Figure 10, we observe that the Er^{3+} peak intensity increases with increasing Er^{3+} ion concentration from 0.02 at% to 0.03 at%. Beyond 0.03 at% of Er^{3+} ion concentration, the Er^{3+} peak intensity decreases. This concentration quenching of Er^{3+} emission can be explained by the energy transfer between neighbouring Er^{3+} ions (Polman & Veggel, 2004). With increasing number of Er^{3+} ions, the mean distance between Er^{3+} ions is reduced. One Er^{3+} ion can de-excite non-radiatively and excite a neighbouring Er^{3+} ion. This process will continue until the energy arrives at a non-radiative defect site in the samples where the energy is given-up non-radiatively (Polman & Veggel, 2004).

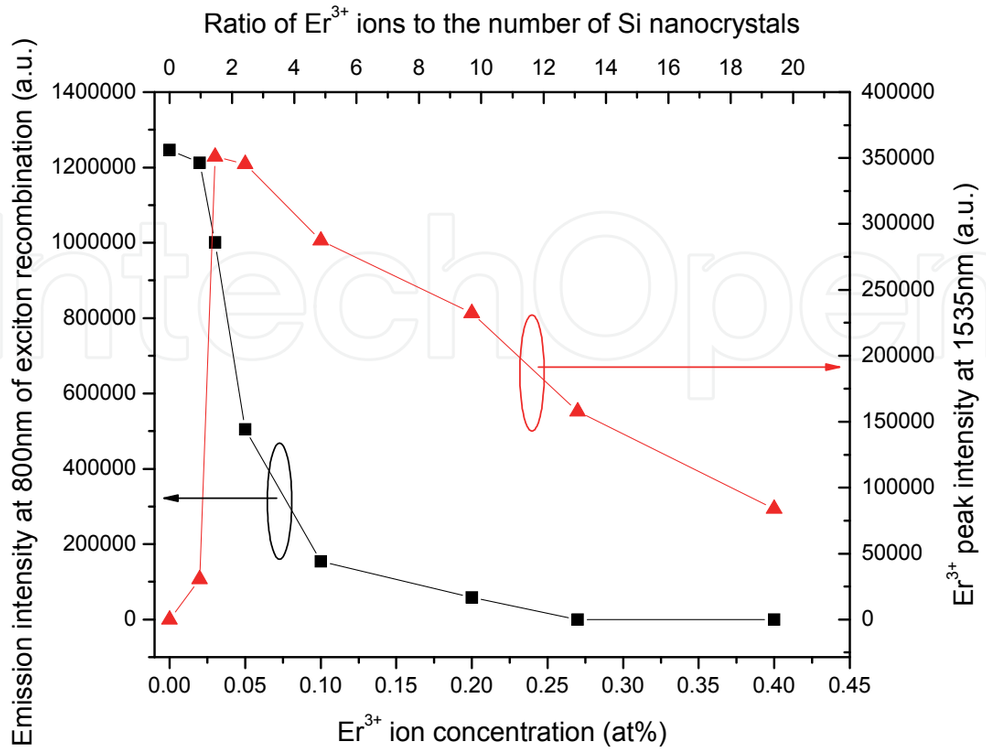

Fig. 10. Variation of the emission intensity at 800nm of the exciton recombinations in Si nanocrystals and the Er^{3+} peak intensity at 1535nm as a function of the Er^{3+} ion concentration and the ratio of Er^{3+} ions to the number of Silicon nanocrystals

As shown in Figure 10, the optimum Er^{3+} peak intensity is obtained at the Er^{3+} ion concentration of 0.03%, which corresponds to the ratio of Er^{3+} ions to the number of Silicon nanocrystals of 1.6. These optimum values of Er^{3+} ion concentration and Er^{3+} ions to Si nanocrystal ratio is comparable to optimum values suggested by Polman & Veggel of 0.02-0.04 at% and 1-2 Er^{3+} ions per Si nanocrystal (Polman & Veggel, 2004). It is noteworthy that the optimum values suggested by Polman & Veggel were derived from the excitation rates of Er^{3+} ions and excitons in Si nanocrystals, both calculated using rise time and decay time of the respective species. In our work, we obtain the optimum Er^{3+} ions to Si nanocrystal ratio from the Er^{3+} emission intensity behaviour.

We see that at the optimum Er^{3+} ion concentration of 0.03 at%, the emission from exciton recombination in Si nanocrystals can still be observed. In this case, the energy transfer from the exciton recombinations in Si nanocrystal to Er^{3+} ions is not fully utilized. One way to fully utilize the Si nanocrystals is to deposit Er^{3+} ions at and near the Er^{3+}:SRO/SiO_2 interface. It is understood that in our superlattice structure, the Si nanocrystals formed may have diameter larger than the thickness of deposited Er^{3+}:SRO layers (see Figure 3 (c)). Hence, when Er^{3+} ions is only deposited in SRO layers, certain areas of the nanocrystals that are in SiO_2 layers will not have any Er^{3+} ions in their vicinity. By depositing Er^{3+} ions at and near the Er^{3+}:SRO/SiO_2 interface, the chance of having Er^{3+} ions near to Si nanocrystals will be improved without the need of increasing Er^{3+} ion concentration in SRO layers.

4.2 Determination of energy transfer rate from the exciton recombinations in Si nanocrystals to Er^{3+} ions

From the previous discussion, when the Er^{3+} ion concentration increases, the coupling between Si nanocrystals and Er^{3+} ions becomes stronger. With stronger coupling, we can expect the energy transfer rate and energy transfer efficiency to increase. Through lifetime measurement, transfer rate as well as transfer efficiency can be deduced. The lifetime measurements were carried out by measuring the emission intensity as a function of time at room temperature. Figure 11 shows the normalized emission decay intensity of the exciton recombinations in Si nanocrystals at 800nm as a function of time of the SRO/SiO_2 and Er^{3+}:SRO/SiO_2 superlattice samples with different Er^{3+} ion concentration.

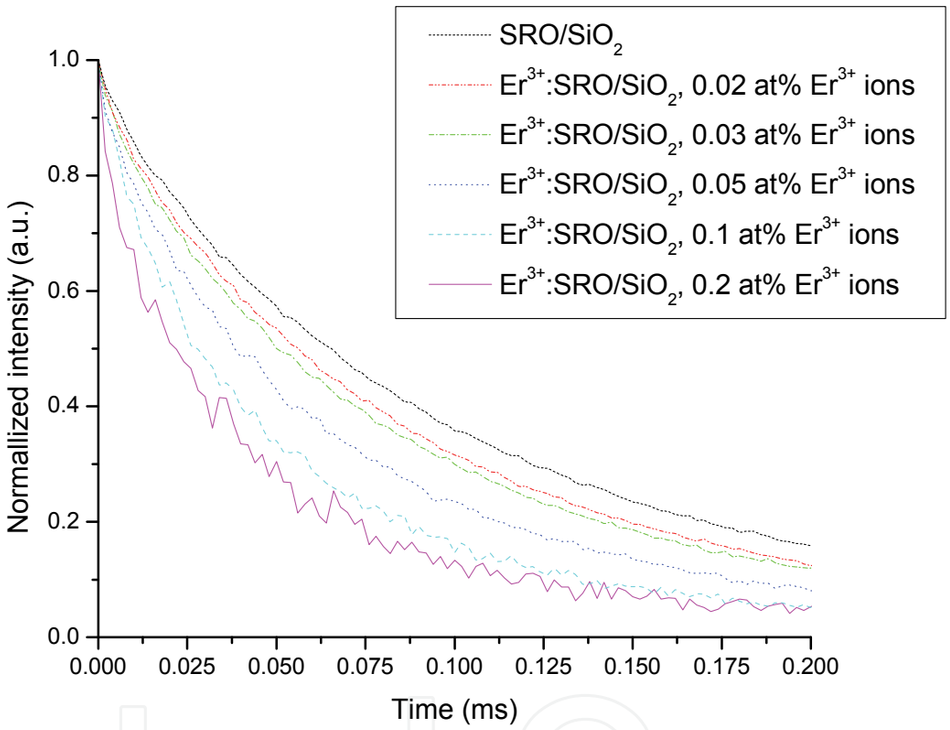

Fig. 11. Normalized room temperature luminescence decay intensity of the exciton recombinations in Si nanocrystals at 800nm of the SRO/SiO_2 and Er^{3+}:SRO/SiO_2 superlattice samples with different Er^{3+} ion concentration

For the samples with Er^{3+} ion concentration larger than 0.2 at%, the emission intensities of exciton recombinations in Si nanocrystals are too low to be measured. The decay curves are well described by stretched exponential decay model (Williams & Watts, 1970):

$$I_{exciton}(t) = I_0 e^{-\left(\frac{t}{\tau_{exciton}}\right)^{\beta}} \quad (1)$$

where $I_{exciton}(t)$ is the intensity of the exciton recombinations in Si nanocrystals measured at time t, I_0 is the intensity of the exciton recombination at time t=0, $\tau_{exciton}$ is the lifetime of the

excitons in Si nanocrystals and β is the stretching exponential coefficient. The value of β ranges from 0 to 1. In the ideal case where species in the material system (Si nanocrystals and Er^{3+} ions) are not interacting with each other, the value of β is equal to 1. In a material system with interacting species, the value of β is less than 1 (Brongersma et al., 1998). Applying equation (1) to the decay curves in Figure 11, we obtained the values of the $\tau_{exciton}$ and β. For our samples, the exciton lifetime in Si nanocrystals decreases from 99.5μs for the SRO/SiO_2 sample to 87μs for the Er^{3+}:SRO/SiO_2 sample with 0.02 at% Er^{3+} ions and then gradually down to 37μs when Er^{3+} ion concentration increases from 0.02 at% to 0.2 at%. The exciton lifetime of each sample is presented in Figure 13 (a) below.

The stretching exponential coefficient β was found to decrease consistently from 0.87 to 0.73 for the SRO/SiO_2 sample, and the Er^{3+}:SRO/SiO_2 samples with Er^{3+} ion concentration increasing from 0.02 at% to 0.2 at%. The decreasing values of β with increasing Er^{3+} ion concentration is consistent with our expectation that the interactions between Si nanocrystals and Er^{3+} ions becomes stronger with increasing Er^{3+} ion concentrations.

Figure 12 shows a simplified energy band diagram of one Si nanocrystal with possible recombination paths.

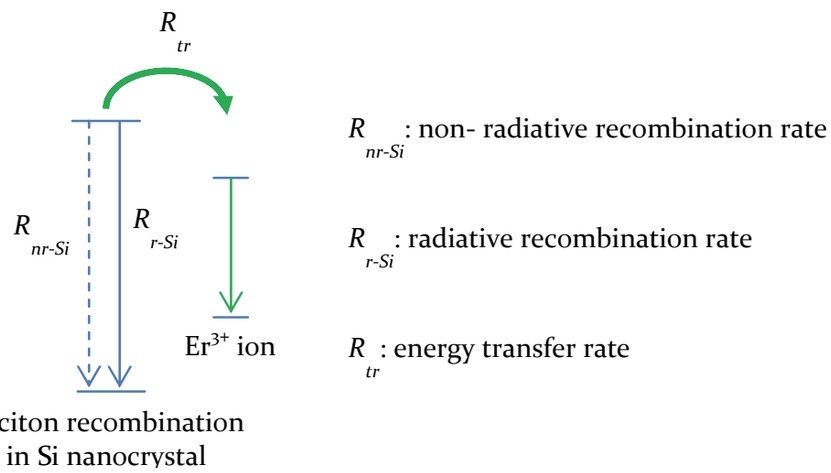

Fig. 12. Possible recombination paths of one Si nanocrystal

Even with our optimum annealing treatment (1050°C annealing in N_2 and passivated for 1 hour), which reduces majority of the defects, there may be still some defects left in the samples that creates non-radiative recombination paths, therefore we incorporate the non-radiative transitions in the exciton recombinations in Si nanocrystals. In the absence of Er^{3+} ions (i.e. for the SRO/SiO_2 samples), the excitons in Si nanocrystals can de-excite through radiative emission or non-radiative recombination. The exciton lifetime, $\tau_{exciton}$, can then be expressed as (Heitmann et al., 2003):

$$\frac{1}{\tau_{exciton}} = R_{nr-Si} + R_{r-Si} \tag{2}$$

where $R_{nr\text{-}Si}$ is the non-radiative recombination rate, and $R_{r\text{-}Si}$ is the radiative recombination rate of excitons. In the presence of Er^{3+} ions (i.e. for the Er^{3+}:SRO/SiO_2 samples), the exciton lifetime, $\tau_{exciton}$, becomes (Heitmann et al., 2003):

$$\frac{1}{\tau_{exciton}} = R_{nr-Si} + R_{r-Si} + R_{tr} \tag{3}$$

where R_{tr} is the energy transfer rate from an exciton to Er^{3+} ions. The transfer rate, R_{tr}, can then be calculated by subtracting the values of $(1/\tau_{exciton})$ in equation (3) to that in equation (2).

Using the values of R_{tr} and $(1/\tau_{exciton})$ in equation (3), the transfer efficiency E_T of our samples can be calculated according to (Heitmann et al., 2003; Savchyn et al., 2007):

$$E_T = \frac{R_{tr}}{R_{nr-Si} + R_{r-Si} + R_{tr}} \tag{4}$$

Figure 13 (a) shows the exciton lifetime, $\tau_{exciton}$, and the transfer rate, R_{tr}, and Figure 13 (b) shows the transfer efficiency, E_T, of our samples.

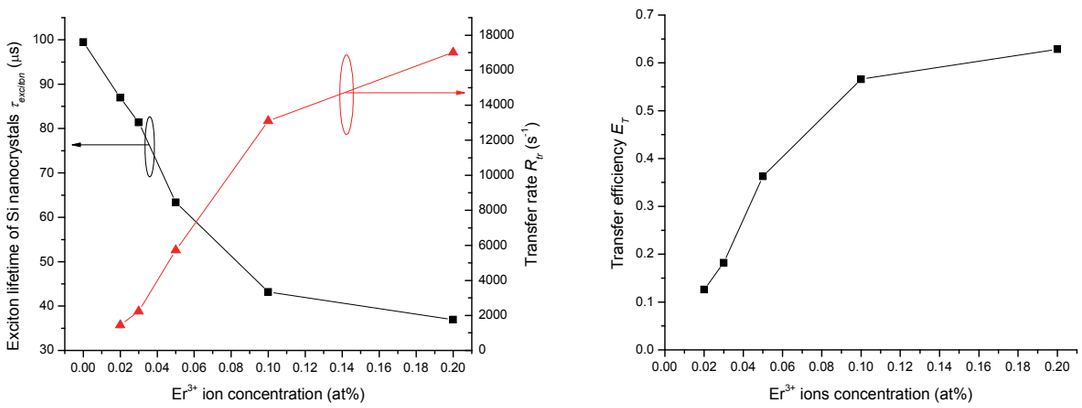

(a) (b)

Fig. 13. (a) Exciton lifetime in Si nanocrystals, $\tau_{exciton}$, transfer rate, R_{tr}, and (b) transfer efficiency, E_T, from the exciton recombinations in Si nanocrystals to Er^{3+} ions as a function of the Er^{3+} ion concentration

As mentioned earlier, when more Er^{3+} ions are incorporated into the samples, the energy transfer rate and transfer efficiency is expected to increase. Indeed, the transfer rate increases from $1.5\times10^{-3}s^{-1}$ to $1.7\times10^{-4}s^{-1}$ (see Figure 13(a)) and transfer efficiency increases from 12% to 63% (see Figure 13 (b)) when Er^{3+} ion concentration increases from 0.02 at% to 0.2 at%. The transfer rate of our material system ranges from $10^{3}s^{-1}$ to $10^{4}s^{-1}$, which is lower than reported values of $10^{4}s^{-1}$ to $10^{5}s^{-1}$ by other groups (Fujii et al., 2004; Savchyn et al., 2007). At this moment, this difference in the energy transfer rate is not obvious to us. We would like to point it out, however, that we have used the superlattice structure, while Fujii et al. and Savchyn et al. were adopting a bulk structure.

As shown in Figure 13 (b), at the optimized Er^{3+} ion concentration of 0.03 at%, the transfer efficiency of our sample is only 18%. Savchyn et al. reported a transfer efficiency of ~60%-75% at Er^{3+} ion concentration of 0.63 at% (Savchyn et al., 2007) and Kik et al reported a transfer efficiency of ~55% at Er^{3+} ion concentration of 1.8 at% (Kik et al., 2000). It is important to note that the transfer efficiency of our sample can reach 63% at the Er^{3+} ion

concentration of 0.2 at%. However, at the Er^{3+} ion concentration of 0.2 at%, Er^{3+} concentration quenching has already taken place and the resulting Er^{3+} emission is not optimized. It is also noteworthy that at our optimized Er^{3+} ion concentration of 0.02 at% and optimized heat treatment (1050°C annealing and passivated), Er^{3+} emission from the superlattice sample is more than 2 times higher than that from the bulk sample (see, respectively, green and red curves in Figure 8(b)). The superlattice structure is showing great potential and optimization can be done to enhance Er^{3+} emission from this material structure.

5. Conclusion

In this chapter, through the PL study of the as-annealed and passivated bulk SRO, Er^{3+}:SRO, SRO/SiO_2, and Er^{3+}:SRO/SiO_2 superlattice samples, 4 different energy transitions and their energy transfer to Er^{3+} ions have been identified and investigated:

1. Radiative energy transition which corresponds to the exciton recombinations in Si nanocrystals. In our material system, the energy transfer due to the exciton recombinations is the most efficient energy transfer both in the bulk Er^{3+}:SRO and Er^{3+}:SRO/SiO_2 superlattice samples.
2. Radiative energy transitions associated with structural defects in bulk samples. The efficiency of the energy transfer due to this type of transitions is lower than that due to the exciton recombinations in Si nanocrystals.
3. Radiative energy transitions associated with structural defects in superlattice samples. These defect transitions give a different PL spectrum than those associated with the defects in the bulk samples and show no energy transfer to Er^{3+} ions.
4. Non-radiative energy transitions due to the dangling bond de-excitation, which quenches other radiative transitions. The non-radiative dangling bond de-excitations have some energy transfer to Er^{3+} ions. The efficiency of this energy transfer is less efficient compared to that due to the exciton recombinations in Si nanocrystals and the transition associated with structural defects in the bulk Er^{3+}:SRO samples. The dangling bonds can effectively be removed by annealing in forming gas environment.

In our study, we have found that the exciton recombinations in Si nanocrystals in our Er^{3+}:SRO/SiO_2 superlattice samples are the most efficient in transferring the energy to Er^{3+} ions. Er^{3+} emission by the exciton recombinations in Si nanocrystals energy transfer from the superlattice samples is more than 2 times higher than that from the bulk samples; while the Er^{3+} emission by the exciton recombination in Si nanocrystals energy transfer in the bulk samples is up to ~2 times higher than Er^{3+} emission by the energy transfer from structural defects in the bulk samples.

Using the superlattice structure at the optimized annealing condition (1050°C RTP followed by passivation), Er^{3+} emissions as a function of Er^{3+} ion concentrations have also been investigated. The optimum concentration of Er^{3+} ions in this material system is 0.03 at%, corresponding to a ratio of Er^{3+} ions to the number of Silicon nanocrystals of 1.6 to 1, achieved at the Er_2O_3 deposition power of 10W.

Through the lifetime study, transfer rate and transfer efficiency by exciton recombinations in Si nanocrystals in the superlattice structure have been determined. The transfer rate ranges from $10^3 s^{-1}$ to $10^4 s^{-1}$. The transfer efficiency can reach 63%, but at optimized Er^{3+} ion concentration of 0.03 at%, the transfer efficiency is 18%. One way to improve the transfer

rate and transfer efficiency is to optimize the Si nanocrystal by incorporate Er^{3+} ions at and near the Er:SRO/SiO_2 interface.

6. References

Brongersma, M. L.; Polman, A.; Min, K. S.; Boer, E.; Tambo, T. & Atwater, H. A. (1998). Tuning the emission wavelength of Si nanocrystals in SiO2 by oxidation. *Applied Physics Letters*, Vol. 72, No. 20, 2577-2579, 00036951 (ISSN)

Bulutay, C. (2007). Electronic structure and optical properties of silicon nanocrystals along their aggregation stages. *Physica E: Low-Dimensional Systems and Nanostructures*, Vol. 38, No. 1-2, 112-117, 13869477 (ISSN)

Castagna, M. E.; Coffa, S.; Monaco, M.; Caristia, L.; Messina, A.; Mangano, R. & Bongiorno, C. (2003). Si-based materials and devices for light emission in silicon. *Physica E: Low-Dimensional Systems and Nanostructures*, Vol. 16, No. 3-4, 547-553, 13869477 (ISSN)

Castagna, M. E.; Muscara, A.; Leonardi, S.; Coffa, S.; Caristia, L.; Tringali, C. & Lorenti, S. (2006). Si-based erbium-doped light-emitting devices. *Journal of Luminescence*, Vol. 121, No. 2 SPEC. ISS., 187-192, 00222313 (ISSN)

Charvet, S.; Madelon, R.; Gourbilleau, F. & Rizk, R. (1999). Spectroscopic ellipsometry analyses of sputtered Si/SiO2 nanostructures. *Journal of Applied Physics*, Vol. 85, No. 8 I, 4032-4039, 00218979 (ISSN)

Fujii, M.; Imakita, K.; Watanabe, K. & Hayashi, S. (2004). Coexistence of two different energy transfer processes in SiO2 films containing Si nanocrystals and Er. *Journal of Applied Physics*, Vol. 95, No. 1, 272-280, 00218979 (ISSN)

Gourbilleau, F.; Portier, X.; Ternon, C.; Voivenel, P.; Madelon, R. & Rizk, R. (2001). Si-rich/SiO2 nanostructured multilayers by reactive magnetron sputtering. *Applied Physics Letters*, Vol. 78, No. 20, 3058-3060, 00036951 (ISSN)

Heitmann, J.; Schmidt, M.; Zacharias, M.; Timoshenko, V. Y.; Lisachenko, M. G. & Kashkarov, P. K. (2003). Fabrication and photoluminescence properties of erbium doped size-controlled silicon nanocrystals. *Materials Science and Engineering B: Solid-State Materials for Advanced Technology*, Vol. 105, No. 1-3, 214-220, 09215107 (ISSN)

Iacona, F.; Irrera, A.; Franzo, G.; Pacifici, D.; Crupi, I.; Miritello, M.; Presti, C. D. & Priolo, F. (2006). Silicon-based light-emitting devices: Properties and applications of crystalline, amorphous and er-doped nanoclusters. *IEEE Journal on Selected Topics in Quantum Electronics*, Vol. 12, No. 6, 1596-1605, 1077260X (ISSN)

Kahler, U. & Hofmeister, H. (2002). Size evolution and photoluminescence of silicon nanocrystallites in evaporated SiOx thin films upon thermal processing. *Applied Physics A: Materials Science and Processing*, Vol. 74, No. 1, 13-17, 09478396 (ISSN)

Kapaklis, V.; Politis, C.; Poulopoulos, P. & Schweiss, P. (2005). Photoluminescent Si nanoparticles embedded in silicon oxide matrix. *Materials Science and Engineering B: Solid-State Materials for Advanced Technology*, Vol. 124-125, No. SUPPL., 475-478, 09215107 (ISSN)

Kik, P. G.; Brongersma, M. L. & Polman, A. (2000). Strong exciton-erbium coupling in Si nanocrystal-doped SiO2. *Applied Physics Letters*, Vol. 76, No. 17, 2325-2327, 00036951 (ISSN)

Kik, P. G. & Polman, A. (2001). Exciton-erbium energy transfer in Si nanocrystal-doped SiO2. *Materials Science and Engineering B: Solid-State Materials for Advanced Technology*, Vol. 81, No. 1-3, 3-8, 09215107 (ISSN)

Polman, A. & van Veggel, F. C. J. M. (2004). Broadband sensitizers for erbium-doped planar optical amplifiers: Review. *Journal of the Optical Society of America B: Optical Physics*, Vol. 21, No. 5, 871-892, 07403224 (ISSN)

Savchyn, O.; Ruhge, F. R.; Kik, P. G.; Todi, R. M.; Coffey, K. R.; Nukala, H. & Heinrich, H. (2007). Luminescence-center-mediated excitation as the dominant Er sensitization mechanism in Er-doped silicon-rich Si O2 films. *Physical Review B - Condensed Matter and Materials Physics*, Vol. 76, No. 19, 10980121 (ISSN)

Savchyn, O.; Kik, P. G.; Todi, R. M. & Coffey, K. R. (2008). Effect of hydrogen passivation on luminescence-center-mediated Er excitation in Si-rich SiO2 with and without Si nanocrystals. *Physical Review B - Condensed Matter and Materials Physics*, Vol. 77, No. 20, 10980121 (ISSN)

Seino, K.; Bechstedt, F. & Kroll, P. (2009). Influence of SiO2 matrix on electronic and optical properties of Si nanocrystals. *Nanotechnology*, Vol. 20, No. 13, 09574484 (ISSN)

Shimizu-Iwayama, T.; Hole, D. E. & Townsend, P. D. (1999). Optical properties of interacting Si nanoclusters in SiO2 fabricated by ion implantation and annealing. *Nuclear Instruments and Methods in Physics Research, Section B: Beam Interactions with Materials and Atoms*, Vol. 147, No. 1-4, 350-355, 0168583X (ISSN)

Silalahi, S. T. H.; Yang, H. Y.; Pita, K. & Mingbin, Y. (2009). Rapid thermal annealing of sputtered silicon-rich oxide/SiO2 superlattice structure. *Electrochemical and Solid-State Letters*, Vol. 12, No. 4, 10990062 (ISSN)

Silalahi, S. T. H.; Vu, Q. V.; Yang, H. Y.; Pita, K. & Mingbin, Y. (2010). Size control of Si nanocrystals by two-step rapid thermal annealing of sputtered Si-rich oxide/SiO2 superlattice. *Applied Physics A: Materials Science and Processing*, Vol. 98, No. 4, 867-871, 09478396 (ISSN)

Silalahi, S. T. H.; Chen, R.; Vu, Q. V.; Pita, K.; Sun, H. D. & Mingbin, Y. (2010). The Effects of Rapid Annealing and Passivation of Co-sputtered Erbium doped Si-rich Oxide/SiO2 Superlattice Structures. *Photonics Global Conference 2010*, Singapore, 14-16 December 2010

Takagahara, T. & Takeda, K. (1992). Theory of the quantum confinement effect on excitons in quantum dots of indirect-gap materials. *Physical Review B*, Vol. 46, No. 23, 15578-15581, 01631829 (ISSN)

Wilkinson, A. R. & Elliman, R. G. (2003). Kinetics of H2 passivation of Si nanocrystals in SiO2. *Physical Review B - Condensed Matter and Materials Physics*, Vol. 68, No. 15, 1553021-1553028, 01631829 (ISSN)

Williams, G. & Watts, D. C. (1970). Non-symmetrical dielectric relaxation behaviour arising from a simple empirical decay function. *Transactions of the Faraday Society*, Vol. 66, No., 80-85, 0014-7672

Wolkin, M. V.; Jorne, J.; Fauchet, P. M.; Allan, G. & Delerue, C. (1999). Electronic states and luminescence in porous silicon quantum dots: The role of oxygen. *Physical Review Letters*, Vol. 82, No. 1, 197-200, 00319007 (ISSN)

Zacharias, M.; Heitmann, J.; Scholz, R.; Kahler, U.; Schmidt, M. & Blasing, J. (2002). Size-controlled highly luminescent silicon nanocrystals: A SiO/SiO2 superlattice approach. *Applied Physics Letters*, Vol. 80, No. 4, 661, 00036951 (ISSN)

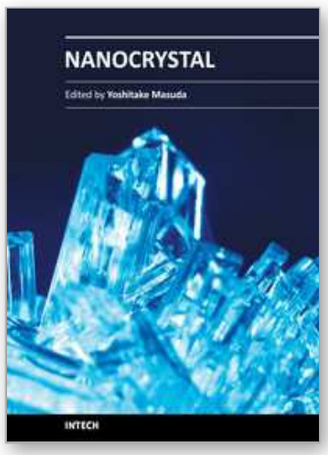

Nanocrystal

Edited by Dr. Yoshitake Masuda

ISBN 978-953-307-199-2
Hard cover, 494 pages
Publisher InTech
Published online 28, June, 2011
Published in print edition June, 2011

We focused on cutting-edge science and technology of Nanocrystals in this book. â€œNanocrystalâ€ is expected to lead to the creation of new materials with revolutionary properties and functions. It will open up fresh possibilities for the solution to the environmental problems and energy problems. We wish that this book contributes to bequeath a beautiful environment and valuable resources to subsequent generations.

How to reference

In order to correctly reference this scholarly work, feel free to copy and paste the following:

Kantisara Pita and Quang Vinh Vu (2011). Energy Transfer from Silicon Nanocrystals to Er3+ Ions Embedded in Silicon Oxide Matrix, Nanocrystal, Dr. Yoshitake Masuda (Ed.), ISBN: 978-953-307-199-2, InTech, Available from: http://www.intechopen.com/books/nanocrystal/energy-transfer-from-silicon-nanocrystals-to-er3-ions-embedded-in-silicon-oxide-matrix

INTECH
open science | open minds

InTech Europe
University Campus STeP Ri
Slavka Krautzeka 83/A
51000 Rijeka, Croatia
Phone: +385 (51) 770 447
Fax: +385 (51) 686 166
www.intechopen.com

InTech China
Unit 405, Office Block, Hotel Equatorial Shanghai
No.65, Yan An Road (West), Shanghai, 200040, China
中国上海市延安西路65号上海国际贵都大饭店办公楼405单元
Phone: +86-21-62489820
Fax: +86-21-62489821

IntechOpen